Citation: Molecular Therapy — Oncolytics (2015) **2,** 15009; doi:10.1038/mto.2015.9

www.nature.com/mto

ARTICLE

Intratumoral INF-γ triggers an antiviral state in GL261 tumor cells: a major hurdle to overcome for oncolytic vaccinia virus therapy of cancer

Christina Kober[1], Stephanie Weibel[1,2], Susanne Rohn[1], Lorenz Kirscher[1] and Aladar A Szalay[1,3–5]

Oncolytic vaccinia virus (VACV) therapy is an alternative treatment option for glioblastoma multiforme. Here, we used a comparison of different tumor locations and different immunologic and genetic backgrounds to determine the replication efficacy and oncolytic potential of the VACV LIVP 1.1.1, an attenuated wild-type isolate of the Lister strain, in murine GL261 glioma models. With this approach, we expected to identify microenvironmental factors, which may be decisive for failure or success of oncolytic VACV therapy. We found that GL261 glioma cells implanted subcutaneously or orthotopically into Balb/c athymic, C57BL/6 athymic, or C57BL/6 wild-type mice formed individual tumors that respond to oncolytic VACV therapy with different outcomes. Surprisingly, only Balb/c athymic mice with subcutaneous tumors supported viral replication. We identified intratumoral IFN-γ expression levels that upregulate MHCII expression on GL261 cells in C57BL/6 wild-type mice associated with a non-permissive status of the tumor cells. Moreover, this IFN-γ-induced tumor cell phenotype was reversible.

Molecular Therapy — Oncolytics (2015) **2**, 15009; doi:10.1038/mto.2015.9; published online 24 June 2015

INTRODUCTION

Glioblastoma multiforme (GBM) is one of the most malignant forms of brain cancer (WHO grade IV) and also the most frequent type of glioma in adults.[1,2] The standard of care for GBM is surgical resection, followed by radiation and temozolomide chemotherapy.[2] In spite of extensive research effort, the disease is still incurable and the prognosis is very poor with a median survival of less than 15 months.[2] Difficulties associated with treatment of GBM are the highly aggressive and infiltrative nature of the tumor into the brain parenchyma. In addition, the histological heterogeneity of the tumor mass, the location of the neoplasm within the brain, the infiltration of the tumor with microglia/macrophages, and the function and morphology of the blood-brain barrier aggravate the therapy.[2–4]

There is a broad range of alternative treatment options presently studied in preclinical and also clinical trials for GBM.[4–6] One of those is oncolytic virotherapy, defined as the use of replication-competent viruses that selectively infect, replicate in and destroy cancer cells while leaving healthy, nontransformed cells and tissues unharmed.[7]

Vaccinia virus (VACV) is a favorable candidate for oncolytic virotherapy due to its safety profile demonstrated during its use as a vaccine in the immunization against smallpox and as double-stranded DNA virus with the unique characteristic to replicate in the cytoplasm only, without integrating into the host genome.[8,9] The efficient killing of tumor cells by recombinant VACVs or VACV wild-type isolates was demonstrated in different tumor xenograft models including a GBM model.[10–13] There is a number of oncolytic viruses tested against malignant gliomas in phase 1 and phase 1/2 clinical trials, *e.g.*, Herpes simplex virus[1], adenovirus, reovirus, Newcastle disease virus, and measles virus.[14,15] The application of those replication-competent viruses was generally safe, however, their antitumor effects observed in the preclinical studies need to be confirmed in human patients.[14,15] One successful approach for oncolytic virotherapy may be the concept of personalized medicine, the screening of cancer patients for best treatment options and thereby maximizing therapeutic outcome.[16,17] Therefore, the identification of biomarkers to locate patients that respond to a particular therapy is paramount.[18,19]

Cancer formation is associated with a close interaction of malignant tumor cells and the tumor microenvironment.[17,19] The amount and composition of infiltrating immune cells varies in different cancer types and in individual patients and is investigated as biomarker in several studies, highlighting the link between the immune status of a tumor and the clinical outcome.[19,20] In addition to cellular interactions, soluble factors released from cells in the micromilieu or from tumor cells control tumor-host interactions.[17,21]

Possible mechanisms resulting in a diverse immune cell infiltration and activation of a particular tumor microenvironment are reviewed by Ascierto *et al.*[22] and include the genetic background

[1]Department of Biochemistry, Biocenter, University of Wuerzburg, Wuerzburg, Germany; [2]Department of Anesthesia and Critical Care, University Hospital of Wuerzburg, Wuerzburg, Germany; [3]Rudolf Virchow Center for Experimental Biomedicine and Institute for Molecular Infection Biology, University of Wuerzburg, Wuerzburg, Germany; [4]Department of Radiation Medicine and Applied Sciences, Rebecca & John Moores Comprehensive Cancer Center, University of California, San Diego, California, USA; [5]Genelux Corporation, San Diego Science Center, San Diego, California, USA. Correspondence: AA Szalay (szalay@biozentrum.uni-wuerzburg.de)
Received 21 January 2015; accepted 28 April 2015

of the host, genetic polymorphism of cytokine receptors, and the genetics of the tumor itself as potential factors. It is known, that one of the most important determinants in the regulation of immune responses in humans and mice is their genetic background.[23] Two inbred mouse strains are used in this study which are defined as prototypical type 1 T helper (Th1) mouse strain in case of C57BL/6 and type 2 T helper (Th2) mouse strain in case of Balb/c mice.[23–26] Adaptive immune response is divided into Th1/Th2 immune response based on a distinct cytokine secretion pattern: Classical Th1 cytokines are, *e.g.*, interleukin 2 (IL-2), IL-12, interferon-γ (IFN-γ), and tumor necrosis factor alpha (TNF-α) whereas IL-4, 5, 6, 10 are Th2 cytokines.[24] In addition to T-cell response, the innate immune cells, primarily macrophages, also show different characteristics in the two mouse strains used in response to pathogenic stimuli like lipopolysaccharide (LPS).[23,25–27] It is well known, that the outcome of diseases in mice infected with several intracellular pathogens is dependent on the genetic background and the Th1/Th2 balance with IFN-γ as one major factor.[24,26,28]

In this study, we set out to identify microenvironmental differences or factors that decisively influence treatment outcome of oncolytic virotherapy and which may be relevant to affect therapeutic success in human patients. We investigated the oncolytic potential of the VACV LIVP 1.1.1, an attenuated wild-type isolate of the Lister strain, in murine GL261 glioma models in a comparative approach: Specifically, we used immunocompetent C57BL/6 wild-type (wt) mice and immunodeficient mouse strains of different genetic background (C57BL/6 athymic nude and Balb/c athymic nude mice) and also studied the effect of different tumor locations (subcutaneous and orthotopic).

RESULTS

Murine GL261 glioma cells were susceptible to VACV infection and oncolysis in cell culture

Infection of GL261 glioma cells with LIVP 1.1.1 (multiplicity of infection (MOI) 0.1) in cell culture revealed replication capacity of 612 ± 244% within 24 hpi, and 6,272 ± 3,821% at 72 hpi referred to the initial infection dose of the cells which was set 100% (Figure 1a). In addition, LIVP 1.1.1-mediated cell death could be demonstrated in a MTT-cell survival assay with only 20 ± 11% surviving cells (MOI 1.0) or 55 ± 12% (MOI 0.1) at 96 hpi (Figure 1b).

Differences in mouse strains and location of tumors influenced viral replication in GL261 glioma models

Using a comparative approach with different tumor locations, immunocompetent and immunodeficient mouse strains as well as different genetic backgrounds, we set out to analyze the replication efficacy of the VACV LIVP 1.1.1 upon intratumoral injection in murine GL261 glioma models.

Viral replication was assumed as an increase in viral titer compared to the initial injection dose (5×10^6 pfu/mouse) delivered i.t. The results revealed viral replication exclusively in Balb/c athymic mice bearing subcutaneous tumors with $5 \times 10^7 \pm 3 \times 10^7$ pfu/g tissue 1 dpi and $8 \times 10^7 \pm 2 \times 10^7$ pfu/g tissue 7 dpi (Figure 1c). All other mouse models and tumor locations led to a decrease in the LIVP 1.1.1 titers during the observation time course. The replication capacity was 15-fold increased in subcutaneous tumors of Balb/c athymic mice at 7 dpi compared to a 28- and 8-fold decrease of the viral load in C57BL/6 wt mice and C57BL/6 athymic mice tumors, respectively (Figure 1c). Replication was not detected either in Balb/c athymic mice ($1 \times 106 \pm 8 \times 10^5$ pfu/g tissue 7dpi) or in the C57BL/6 wt mice ($6 \times 104 \pm 6 \times 104$ pfu/g tissue 7dpi) with orthotopic brain tumors (Figure 1d). These findings coincide with a 4-fold decrease of the viral load in Balb/c athymic and 100-fold decrease in C57BL/6 wt mice at 7 dpi (Figure 1d).

Intratumoral LIVP 1.1.1 injection into subcutaneous GL261 tumors of Balb/c athymic mice significantly delayed tumor growth

Since major differences in virus replication in the subcutaneous tumors in different mouse strains were detected, we analyzed tumor growth kinetics in response to oncolytic virotherapy of these tumor models. In the LIVP 1.1.1 groups of all three models there was a slight tumor growth delay (Figure 1e–g) but only in Balb/c athymic mice a significant tumor growth delay from 4 dpi to the end of the study was detected (Figure 1e). All tumor models showed a very fast and aggressive tumor growth as mice reached a tumor size of 4,000 mm^3 in 9–14 days.

Major differences in the tumor microenvironment were detectable between immunocompetent wild-type mice and immunodeficient athymic mice

Replication analysis affirmed that the mouse genetic background had a major impact on viral replication in the subcutaneous GL261 tumor models, as both C57BL/6 mouse models (athymic and wt) did not support viral replication, whereas the BALB/c background does. This led us to the question, which additional immunological factors in the tumor microenvironment of the subcutaneous tumor model of Balb/c athymic mice enabled virus replication on the one hand and prevented replication in mice with C57BL/6 background on the other side. We found that the virus titer differed significantly at 1 dpi (Figure 1c) implicating that the differences seem to exist in tumors before virus infection. Therefore, we performed a detailed characterization of tumor microenvironments of the subcutaneous tumor models already on d0.

In a first step, a subset of 59 biomarkers was tested in subcutaneous tumors of five mice of each mouse strain using a mouse immune related antigen profiling. Nineteen biomarkers that showed significant differences in the mouse strains tested are listed in Table 1. The significant differences of the proinflammatory signature were all detectable in the C57BL/6 wt mice compared to both athymic mouse strains (C57BL/6 and Balb/c) but not in the C57BL/6 athymic in comparison to Balb/c athymic mice. In most cases, highest biomarker concentrations were detectable in C57BL/6 wt mice followed by C57BL/6 athymic and Balb/c athymic mice.

The profiling revealed that there was a significant upregulation of proinflammatory cytokines such as interferon-γ-induced protein 10 (IP-10), IL-1α, IL-11 and macrophage inflammatory protein-1β (MIP-1β), and chemoattractants such as monocyte chemotactic protein (MCP)-1, MCP-3, MCP-5 recruiting mainly monocytes, macrophages, lymphocytes, eosinophils, MIP-2, and granulocyte chemoattractant protein-2 (GCP-2) attracting neutrophils and lymphotactin and IP-10 recruiting lymphocytes.[29] Factors responsible for the proinflammatory signature (GCP-2, MIP-1β, MIP-2, MCP-3, and MCP-5) are mainly produced by macrophages. Another factor which was almost fivefold upregulated in the wild-type mice was vascular endothelial growth factor A (VEGF-A) as well as CD40.

In a second experiment, we performed an immune cell profiling of the subcutaneous GL261 tumors at d0 to determine, whether there were major qualitative and/or quantitative differences in the immune cell populations within these tumor models (Table 2). Single cell suspensions of the tumors were prepared and flow

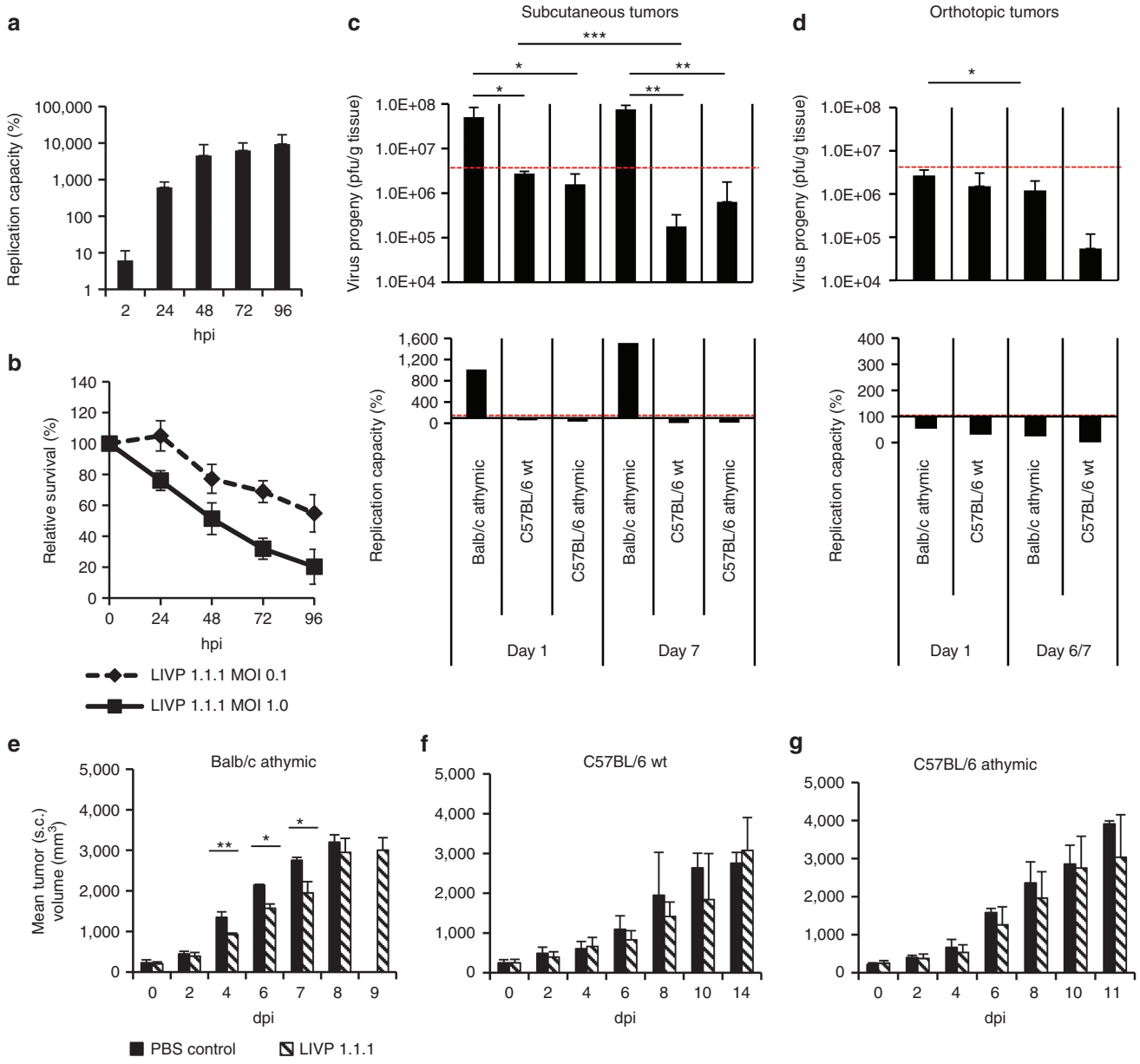

Figure 1 LIVP 1.1.1 replicates only in GL261 tumors implanted subcutaneous (s.c.) into Balb/c athymic mice. Viral replication in GL261 cells and supernatant infected with LIVP 1.1.1 at a multiplicity of infection (MOI) of 0.1 was analyzed by standard viral plaque assay (**a**). The bar chart shows the replication capacity presented as mean values and standard deviation of three independent experiments performed in triplicate. MTT assay (**b**) was performed to detect the percentage of living cells after infection with LIVP 1.1.1 (MOI 0.1, 1.0). Experiments were performed in triplicate and repeated three times in an independent experiment. LIVP 1.1.1 titers calculated as (pfu/g tissue) and replication capacity in (%) at day 1 or 6/7 postinfection in subcutaneous (s.c.) (**c**) or orthotopic (o) (**d**) GL261 tumors implanted in Balb/c athymic, C57BL/6 wt or C57BL/6 athymic mice. Percentages of injected virus dose (5×10^6 pfu/mouse) and viral titers were determined by plaque assay. Each time point represents the mean of at least four mice. Red line demonstrates the level of the virus inoculum of 5×10^6 pfu/mouse. Differences of the virus titers in subcutaneous or orthotopic GL261 tumors were tested between mouse strains at 1 dpi and 6/7 dpi, respectively and within each mouse strain between 1 dpi and 6/7 dpi by using two-sided *t*-test with unequal variances $^*P < 0.05$, $^{**}P < 0.01$, $^{***}P < 0.001$. Balb/c athymic ($n = 3/4$) (**e**), C57BL/6 wt ($n = 5/6$) (**f**), and C57BL/6 athymic ($n = 6$) (**g**) mice with (s.c.) GL261 tumors were injected (i.t.) with 5×10^6 pfu LIVP 1.1.1 or PBS at a tumor volume between 200–400 mm³. Tumor growth (**e–g**) was monitored by measuring the tumor every other day. Depicted are the mean values with standard deviation. Differences between virus treated and PBS treated groups or virus titers were tested using two-sided *t*-test with unequal variances $^*P < 0.05$, $^{**}P < 0.01$, $^{***}P < 0.001$.

cytometry analysis was performed. In the C57BL/6 wt mice besides $CD3^+/CD4^+$ T-lymphocytes, immune cell subsets of the innate immune system such as $CD49^+$ natural killer (NK) cells, $CD11b^+/CD11c^+$ immature myeloid cells and cells of the monocyte/macrophage lineage ($CD45^+/CD11b^+$, $CD11b^+/MHCII^+$, $F4/80^+/MHCII^+$) were significantly upregulated compared to the C57BL/6 athymic and Balb/c athymic mice (Table 2). Flow cytometry analysis of the blood in these mice (Table 2) showed that besides the expected $CD3^+/CD4^+$ and $CD3^+/CD8^+$ T-lymphocytes present exclusively in the wild-type mice, significantly more $CD19^+$ B-lymphocytes, $CD49^+$ NK cells, $CD11b^+/Ly6c^+$ dendritic cells, $CD11b^+/CD11c^+$ immature myeloid cells, and $CD11b^+/Gr1^+$ myeloid-derived suppressor cells (MDSCs) were detected in the C57BL/6 athymic mice compared to the Balb/c athymic mice. In case of $CD49^+$ NK cells and $CD11b^+/$

Table 1 Mouse immune-related protein antigen profiling of C57BL/6 wt, C57BL/6 athymic, and Balb/c athymic mice in GL261 tumors at the day of infection (d0)[a]

			Mouse strains			*P value*		
Biomarker	*Abbr.*	*Unit*	*C57BL/6 wt*	*C57BL/ 6 athymic*	*Balb/ c athymic*	*C57BL/6 wt: Balb/c athymic*	*C57BL/6 wt: C57BL/6 athymic*	*C57BL/6 athymic: Balb/c athymic*
Granulocyte chemotactic protein-2	GCP-2	ng/ml	0.2 ± 0.03	0.1 ± 0.02	0.1 ± 0.01	0.005	0.004	0.220
Interferon-γ-induced protein 10	IP-10	pg/ml	2940.0 ± 602.2	921.0 ± 1123.9	423.0 ± 154.2	0.003	0.007	0.323
Interleukin-1α	IL-1α	pg/ml	1035.5 +/- 123.5	572.5 ± 158.6	438.8 ± 218.3	0.002	0.004	0.266
Interleukin-11	IL-11	pg/ml	101.3 ± 17.9	70.8 ± 6.2	n.d.	—	0.036	—
Leukemia inhibitory factor	LIF	pg/ml	775.0 ± 112.9	533.8 ± 167.1	452.3 ± 71.5	0.006	0.037	0.378
Lymphotactin		pg/ml	879.5 ± 201.4	516.2 ± 267.6	188.0 ± 32.0	0.006	0.053	0.051
Macrophage inflammatory protein-1β	MIP-1β	pg/ml	1457.5 ± 281.2	294.2 ± 164.5	171.0 ± 15.9	0.003	0.001	0.170
Macrophage inflammatory protein-2	MIP-2	pg/ml	34.0 ± 6.6	17.6 ± 4.9	15.3 ± 2.8	0.006	0.007	0.399
Monocyte chemotactic protein 1	MCP-1	pg/ml	436.8 ± 122.1	160.3 ± 51.3	115.8 ± 44.0	0.010	0.014	0.183
Monocyte chemotactic protein 3	MCP-3	pg/ml	320.5 ± 120.9	143.4 ± 64.2	96.8 ± 25.5	0.032	0.053	0.189
Monocyte chemotactic protein-5	MCP-5	pg/ml	184.5 ± 38.9	94.8 ± 38.2	87.6 ± 33.0	0.007	0.012	0.758
T-cell-specific protein RANTES	RANTES	pg/ml	0.3 ± 0.1	0.1 ± 0.1	0.03 ± 0.01	0.017	0.020	0.226
Vascular cell adhesion molecule-1	VCAM-1	ng/ml	47.0 ± 7.5	27.0 ± 4.0	26.6 ± 3.9	0.007	0.007	0.876
Vascular endothelial growth factor A	VEGF-A	pg/ml	9105.0 ± 2539.6	1684.2 ± 829.3	2230.0 ± 600.3	0.011	0.007	0.271
von Willebrand factor	vWF	ng/ml	12.0 ± 2.2	8.6 ± 1.5	8.3 ± 2.3	0.045	0.043	0.805
Stem cell factor	SCF	pg/ml	1380.0 ± 175.7	791.6 ± 237.3	542.8 ± 195.9	0.0003	0.004	0.110
CD40	CD40	pg/ml	724.8 ± 361.3	138.0 ± 51.7	154.6 ± 29.9	0.051	0.046	0.556
Tissue inhibitor of metalloproteinases 1	TIMP-1	ng/ml	10.1 ± 1.3	9.5 ± 1.9	5.9 ± 1.6	0.003	0.654	0.011
Matrix metalloproteinase-9	MMP-9	ng/ml	20.8 ± 5.9	11.0 ± 4.1	6.7 ± 1.7	0.014	0.037	0.075

[a]Shown are the mean values and standard deviation ($n = 5$; C57BL/6 and Balb/c athymic and $n = 4$ C57BL/6 wt). Differences between the mouse strains were analyzed using two-sided *t*-test with unequal variances, $^{*}P < 0.05$ (yellow), $^{**}P < 0.01$ (orange), $^{***}P < 0.001$ (dark orange). Proinflammatory cytokines and chemoattractants are marked in green; modulators of tissue homeostasis are marked in blue.

CD11c^{+} immature myeloid cells, the differences were also significant between C57BL/6 wt and C57BL/6 athymic mice.

This study highlighted that implantation of the same tumor cells in three different mouse strains resulted in a completely different tumor microenvironment with highest differences between immunodeficient and immunocompetent mice. It also demonstrated the influence of the adaptive immune system as main microenvironmental modulator. The comparison of these three mouse strains further revealed a tendency that the C57BL/6 athymic mice might be in an "intermediate state" between C57BL/6 wt and Balb/c athymic mice.

Phagocytic macrophages were excluded as factor responsible for viral clearance in C57BL/6 wt mice

After characterization of the subcutaneous GL261 tumor model in different mouse strains, we tried to elucidate whether therapeutic efficiency in the "non-responder" C57BL/6 wt mice can be improved. As the proinflammatory signature was mainly produced by macrophages (Table 1) which were significantly recruited to subcutaneous GL261 tumors in C57BL/6 wt mice in comparison to athymic mice, we depleted macrophages in C57BL/6 wt mice with clodronate liposomes prior to virus infection. The depletion efficiency was confirmed by flow cytometry analysis with different macrophage marker combinations 1 dpi (Figure 2a–d). Standard viral plaque assay revealed that the virus titer in both groups (PBS and clodronate liposomes) did not differ significantly either on day 1 or on day 7 post infection (Figure 2e). Therefore, macrophages were excluded as factor responsible for the pronounced reduction of viral particles in this model detected already 1 dpi.

Upregulation of MHCII observed on nonmonocytic cells from subcutaneous GL261 tumors in C57BL/6 wt mice at the day of infection

The immunohistochemical analysis of subcutaneous GL261 tumor sections of C57BL/6 wt and athymic as well as Balb/c athymic mice at d0 revealed a significant upregulation of MHCII in the C57BL/6 wt mice (Figure 3a). The upregulation of MHCII in C57BL/6 athymic mice compared to Balb/c athymic mice was not significant. Additionally, amounts of CD68^{+} immune cells were not significantly different in the three mouse strains (Figure 3b). Surprisingly, the expression of the marker MHCII did not colocalize with the immune cell marker CD68 (Figure 3d,e), implicating the existence of a MHCII^{+} non-macrophage population. The expression of MHCII was distributed homogenously throughout the tumor center and at the tumor rim

Table 2 Immune cell profiling and comparison of single cell suspensions isolated from subcutaneous GL261 tumors and blood of C57BL/6 wt, C57BL/6 athymic, and Balb/c athymic mice on d0[a]

Tumor	Marker	C57BL/6 wt	C57BL/6 athymic	Balb/c athymic	C57BL/6 wt: C57BL/6 athymic	C57BL/6 wt: Balb/c athymic	C57BL/6 athymic: Balb/c athymic
Lymphocytes	$CD3^+/CD4^+$	2.4 ± 0.7	< 1	< 1	0.030	0.039	–
	$CD3^+/CD8^+$	< 1	< 1	< 1	–	–	–
	$CD19^+$	2.4 ± 2.0	1.1 ± 0.1	2.5 ± 0.7	0.26	0.71	0.05
NK cells	$CD49b^+$	5.5 ± 0.3	1.9 ± 0.0	4.1 ± 0.6	0.001	0.04	0.01
Dendritic cells	$CD11b^+/Ly6c^+$	5.7 ± 1.7	1.9 ± 0.8	< 1	0.16	0.08	0.09
Immature myeloid cells	$CD11b^+/CD11c^+$	4.7 ± 0.9	3.3 ± 1.1	1.5 ± 0.4	0.04	0.03	0.08
MDSC	$CD11b^+/Gr1^+$	< 1	1.7 ± 0.5	< 1	0.03	–	0.12
Neutrophils	$CD11b^+/Ly6G^+$	< 1	< 1	< 1	–	–	–
Monocytes/	$CD45^+/CD11b^+$	8.8 ± 1.1	3.5 ± 0.1	2.3 ± 0.5	0.01	0.004	0.04
Macrophages	$CD11b^+/MHCII^+$	6.78 ± 0.0	1.9 ± 0.4	<1	0.0002	0.0004	0.03
	$CD68^+/MHCII^+$	3.5 ± 2.0	1.6 ± 0.8	1.0 ± 0.3	0.22	0.16	0.37
	$F4/80^+/MHCII^+$	2.5 ± 0.5	< 1	< 1	0.02	0.01	–
Blood	Marker	C57BL/6 wt	C57BL/6 athymic	Balb/c athymic	C57BL/6 wt: C57BL/6 athymic	C57BL/6 wt:Balb/c athymic	C57BL/6 athymic: Balb/c athymic
	CD3+/CD4+	16.9 ± 3.0	< 1	< 1	0.01	0.01	–
Lymphocytes	CD3+/CD8+	16.9 ± 2.0	< 1	< 1	0.006	0.006	–
	CD19+	52.2 ± 5.0	61.2 ± 1.9	44.6 ± 3.1	0.10	0.01	0.02
NK cells	CD49+	10.0 ± 2.4	29.1 ± 3.0	13.1 ± 0.7	0.001	0.03	0.002
Dendritic cells	CD11b+/Ly6c+	10.2 ± 4.5	15.4 ± 1.7	8.7 ± 2.3	0.05	0.68	0.02
Immature myeloid cells	CD11b+/CD11c+	5.6 ± 1.1	19.3 ± 2.2	4.6 ± 0.8	0.002	0.29	0.003
MDSC	CD11b+/Gr1+	5.5 ± 3.6	12.7 ± 2.1	6.4 ± 2.4	0.05	0.72	0.03
Neutrophils	CD11b+/Ly6G+	6.2 ± 3.6	13.0 ± 1.8	8.2 ± 2.9	0.07	0.51	0.08
Monocytes	CD11b+/MHCII+	4.2 ± 1.3	5.6 ± 1.6	7.0 ± 0.8	0.29	0.06	0.28
Macrophages	F4/80+/MHCII+	1.0 ± 0.2	1.5 ± 0.3	3.3 ± 0.2	0.04	0.002	0.004

[a]Shown are mean and standard deviation of three mice per group in percentages (%). Differences in marker expression between mouse strains were analyzed using two-sided *t*-test with unequal variances $*P < 0.05$ (yellow), $**P < 0.01$ (orange), $***P < 0.001$ (dark orange). Highlighted in red is the mouse strain showing the highest percentage of a particular marker combination. 10,000 events/sample and staining were measured. Percentages below 1% are described as < 1.

(quantification not shown). An upregulation of MHCII on $CD68^-$ cells was observed in C57BL/6 athymic mice with patchy distribution, but not in Balb/c athymic mice (Figure 3c,d). Further, the morphology of the $MHCII^+/CD68^-$ cells was distinct from immune cell populations and resembled that of the GL261 glioma cells. The upregulation of MHCII on the surface of non-immune cells/nonantigen-presenting cells is described especially in the context of malignant gliomas.[30] For further quantification, flow cytometry analysis revealed that in C57BL/6 wt tumors 46 ± 23% were $MHCII^+/CD68^-$ cells whereas in C57BL/6 athymic mice 3 ± 2% and in Balb/c athymic mice no $MHCII^+/CD68^-$ cells could be detected (Figure 3f).

VACV infection did not influence MHCII expression on nonmonocytic cells

Further analysis revealed that intratumoral LIVP 1.1.1 administration had no impact on MHCII expression in the different mouse models 1 dpi with no difference between the LIVP 1.1.1 and PBS groups (Figure 3g). The expression of MHCII positive cells was homogenously scattered throughout tumor center and rim in the C57BL/6 wt mice. The MHCII pattern 1 dpi with strongest MHCII expression in subcutaneous tumors in C57BL/6 wt, followed by C57BL/6 athymic and at least in Balb/c athymic mice was also present 7 dpi (data not shown).

Analysis of orthotopic tumors of C57BL/6 wt mice revealed that 1 and 7 dpi in VACV- and PBS-injected tumors a large proportion of tumor cells expressed MHCII (Figure 3h–j). Tumor cells could be distinguished well from Iba-1-positive microglial cells and from astrocytes (data not shown).

Taken together, these data implicated that expression of MHCII on GL261 tumor cells was not limited to subcutaneous tumors but also occurred in the orthotopic natural location of the tumor within the brains of these mice. Further, it was not a consequence of virus infection but of the tumor microenvironment itself.

Diminished viral replication and MHCII upregulation on GL261 tumor cells in cell cultures upon pretreatment with IFN-γ

In our biomarker profiling, we detected factors such as IP-10, MCP-1 or MIP-1β which were differentially expressed with highest

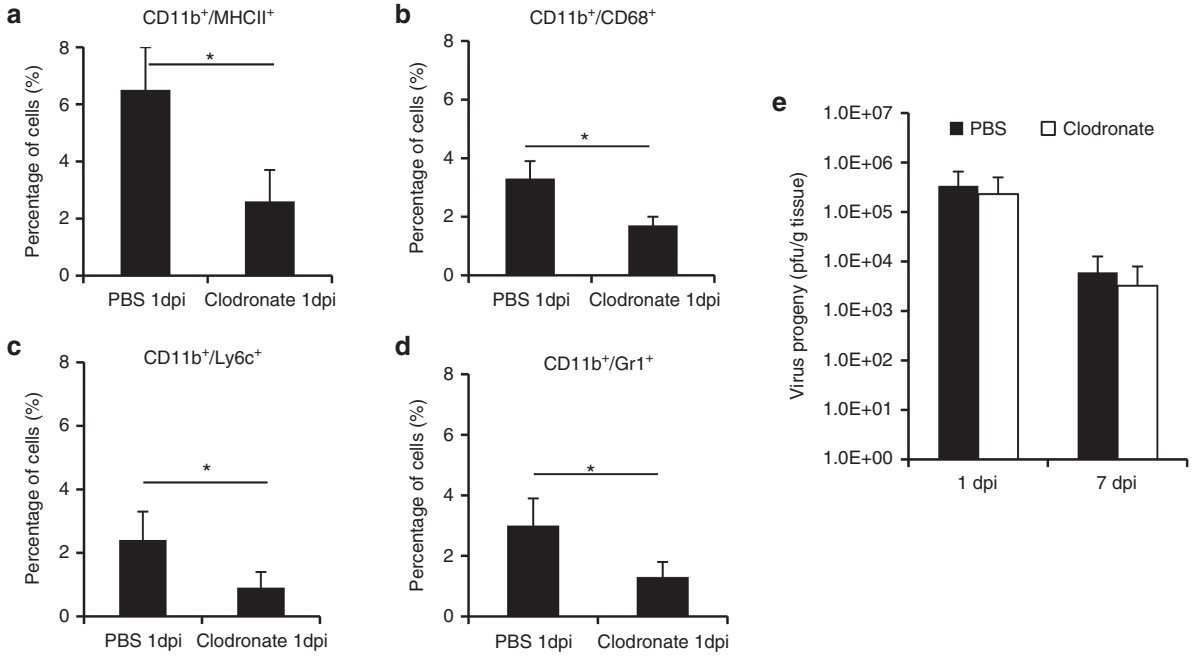

Figure 2 Clodronate depletion did not show an effect on virus replication in C57BL/6 mice with subcutaneous GL261 tumors. C57BL/6mice with subcutaneous GL261 tumors were injected (i.p.) with 200 µl PBS or codronate 3 days before tumor infection. Flow cytometry analysis was performed 1 dpi to confirm the clodronate depletion of monocytes/macrophages (**a–d**). Shown are mean and standard deviation of three mice per group. Viral titers were determined by plaque assay 1 and 7 dpi (**e**). Each time point represents the mean of at least three mice. Significant differences in marker gene expression and viral titers were tested with two-sided t-test with unequal variances.

concentrations in C57BL/6 wt mice, followed by C57BL/6 athymic and Balb/c athymic mice (Table 1). Those correlated very well with the expression levels of MHCII detected in the subcutaneous tumors of all three mouse models (Figure 3c–e). IP-10, MCP-1, or MIP-1β are known to be induced and upregulated by IFN-γ a proinflammatory cytokine with immunomodulatory functions.[31] Further, it is reported that IFN-γ does upregulate MHCII not only on professional APCs for antigen-specific $CD4^+$ T-lymphocyte activation but also on nonprofessional APCs such as tumor/glioma cells that do not express MHCII constitutively.[30–32] We set out to analyze whether this phenotypic change of GL261 tumor cells may have an impact on viral replication or virus-mediated toxicity.

For this, GL261 cells in cell cultures were either stimulated with rm-IFN-γ (10, 30, 60, 100) ng/ml or with rm-IL-4 (10 ng/ml) which are cytokines for induction of M1/M2 phenotypes in macrophages.[33] Indeed, stimulation of GL261 cells with 10 ng/ml IFN-γ for 24 hours resulted in an increased amount of $MHCII^+$ GL261 cells from 0% to 30% ± 3% which increased further to 79 ± 2% at 72 hours post stimulation. Mock (w/o) or IL-4 stimulated cells did not show MHCII expression on their surface (Figure 4a). Expression of MHCII increased over time from 24 to 72 hours after stimulation with IFN-γ and dependent on the dose at various concentrations (10, 30, 60, and 100) ng/ml (Figure 4a). Flow cytometry analysis using propidium iodide (PI) as a marker for cell death revealed that IFN-γ stimulation at a concentration of 10 ng/ml had no effect on cell viability compared to GL261 cells without stimulation (w/o) or stimulated with 10 ng/ml IL-4 at 24 and 72 hours post stimulation (Figure 4b). Seventy-two hours post stimulation, proliferation of IFN-γ stimulated cells was significantly reduced compared to cells (w/o) or IL-4 stimulated (Figure 4b).

Replication analysis in differentially stimulated GL261 tumor cells revealed that cells preincubated with IFN-γ were infected with LIVP 1.1.1 but the virus titers were more than 100-fold lower than cells infected after preincubated with IL-4 or (w/o) (Figure 4c). The detected virus titers (24–72 hpi) of IFN-γ preincubated cells remained below the initial infection dose, implicating that no viral replication occurred in these cells. No difference was detectable between w/o or IL-4 preincubation. Virus-mediated toxicity (MOI 1 and MOI 0.1) was significantly reduced in IFN-γ preincubated cells compared to cells without preincubation with IFN-γ. Seventy-two hours after infection with MOI 0.1 only 21 ± 14% cells survived in the unstimulated samples compared to 94 ± 18% in the IFN-γ stimulated samples (Figure 4d). In summary, these results in cell culture revealed the capacity to upregulate MHCII in the murine glioma cell line GL261 by INF-γ stimulation and highlighted an antiviral state of the $MHCII^+$ GL261 tumor cells.

Impact of endogenous IFN-γ levels in C57BL/6 wt mice on viral infection

To affirm the findings that IFN-γ is responsible for the upregulation of MHCII on the surface of the tumor cells and the reduced viral replication in the C57BL/6 models *in vivo*, we compared viral replication in C57BL/6 wt mice with that of C57BL/6 IFN-γ knockout (KO) mice. Flow cytometry analyses revealed a significantly lower percentage of $MHCII^+/CD11b^-$ or $MHCII^+/F4/80^-$-tumor cells in subcutaneous GL261 tumors of C57BL/6 IFN-γ KO mice compared to C57BL/6 wt mice (Figure 4e,f). Furthermore, the replication capacity of LIVP 1.1.1 was significantly increased in C57BL/6 IFN-γ KO compared to the C57BL/6 wt mice (Figure 4g). These findings confirmed the role of endogenous IFN-γ levels in C57BL/6 wt mice as candidate factor responsible for diminished VACV replication and as factor in charge for upregulation of MHCII on GL261 tumor cells in this particular mouse model.

IFN-γ-induced antiviral state in GL261 glioma cells is reversible

We showed that GL261 tumor cells which are initially in a $MHCII^-$-VACV-permissive status were modified or imprinted into

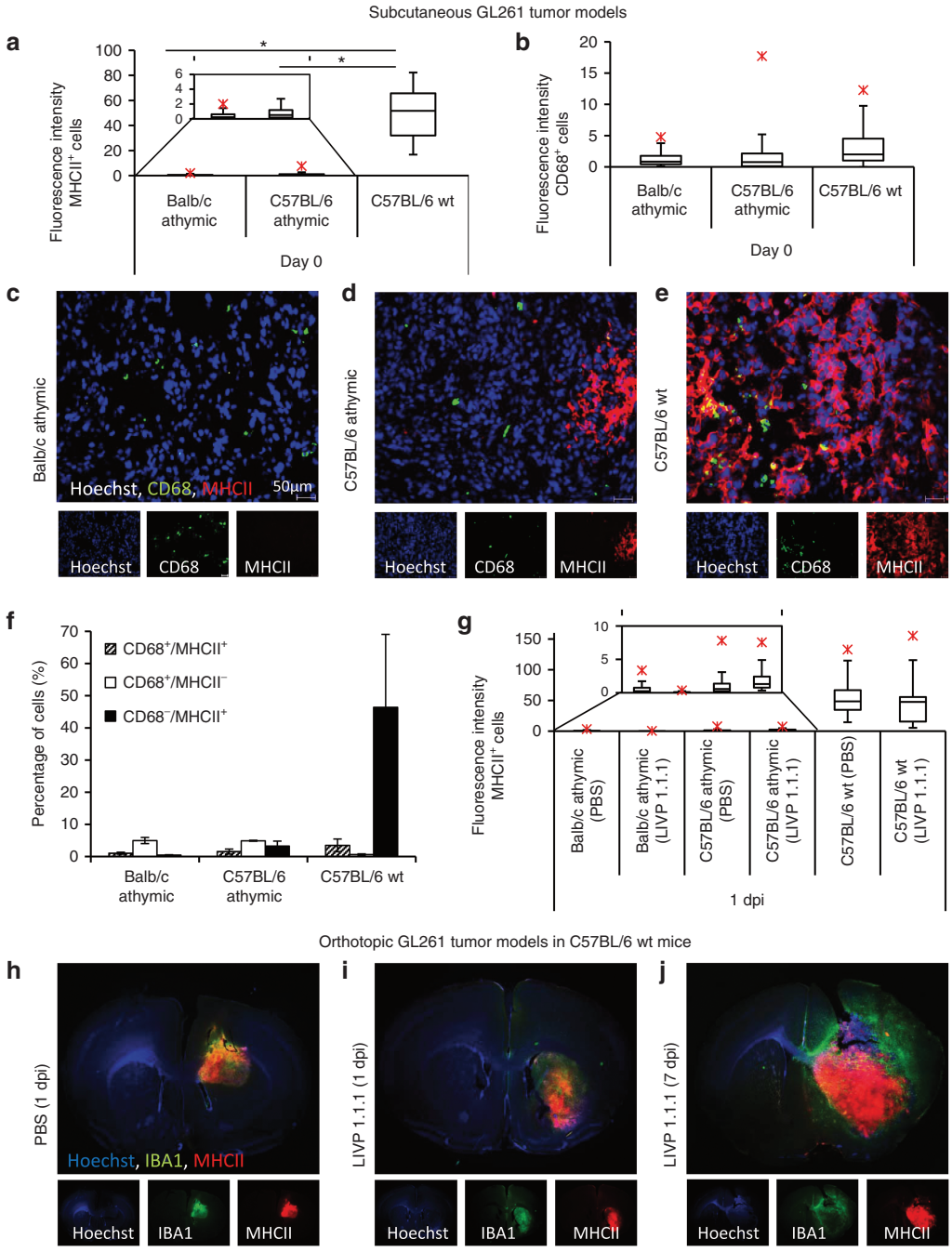

Figure 3 MHCII upregulation on CD11b⁻ cells was independent of VACV infection and tumor location. The fluorescence intensity of MHCII (**a**) and CD68 (**b**) labeled subcutaneous tumor sections (tumor rim and tumor center) was determined in 10 images per tumor ($n = 3$ mice/group) using ImageJ. Depicted are box and whisker charts. Tumor cryosections (10 µm) of Balb/c athymic (**c**) C57BL/6 athymic (**d**) and C57BL/6 wt mice (**e**) on d0 were stained with antibodies against CD68 (green) and MHCII (red). Hoechst 3342 was used to stain cell nuclei (blue). Ten images ($n = 3$ mice/group) were taken in two independent experiments. The images are representative examples. Magnification 20×, scale bar 50 µm. The experiment was performed twice. Percentages of CD68 and MHCII double or single positive cells (**f**) were determined by flow cytometry analysis of single cell suspensions of subcutaneous GL261 tumors on d0 ($n = 3$ mice per group). The bar chart shows mean and standard deviation. The fluorescence intensity of MHCII (**g**) of tumor cryosections (10 µm) of all three mouse models infected (i.t.) with LIVP 1.1.1 or PBS 1 dpi was determined as described for (**a**) Agarose sections (200 µm) of orthotopic GL261 tumors (C57BL/6 wt mice $n = 3$) infected with PBS 1 dpi (**h**) or LIVP 1.1.1 (**i/j**) 1 and 7 dpi, stained with Hoechst (blue) and antibodies against Iba-1 (green) and MHCII (red). The images are representative examples. Staining was performed in duplicate. Differences in fluorescence intensity between mouse strains were tested using two-sided *t*-test with unequal variances, $^{*}P < 0.05$, $^{**}P < 0.01$, $^{***}P < 0.001$.

a MHCII⁺-VACV non-permissive status after implantation into C57BL/6 wt mice. We wanted to elucidate whether this modification of the GL261 tumor cells in C57BL/6 wt mice was a reversible or a permanent effect and therefore, a potential target for improving oncolytic virotherapy in tumors with MHCII signatures.

Hence, single cell suspensions of subcutaneous GL261 tumors from C57BL/6 wt mice were prepared. As controls, GL261 tumors of Balb/c athymic mice were used since the status of those tumor cells was still MHCII⁻-VACV-permissive (Figure 5f). By flow cytometry analysis, we detected a reduction of the number

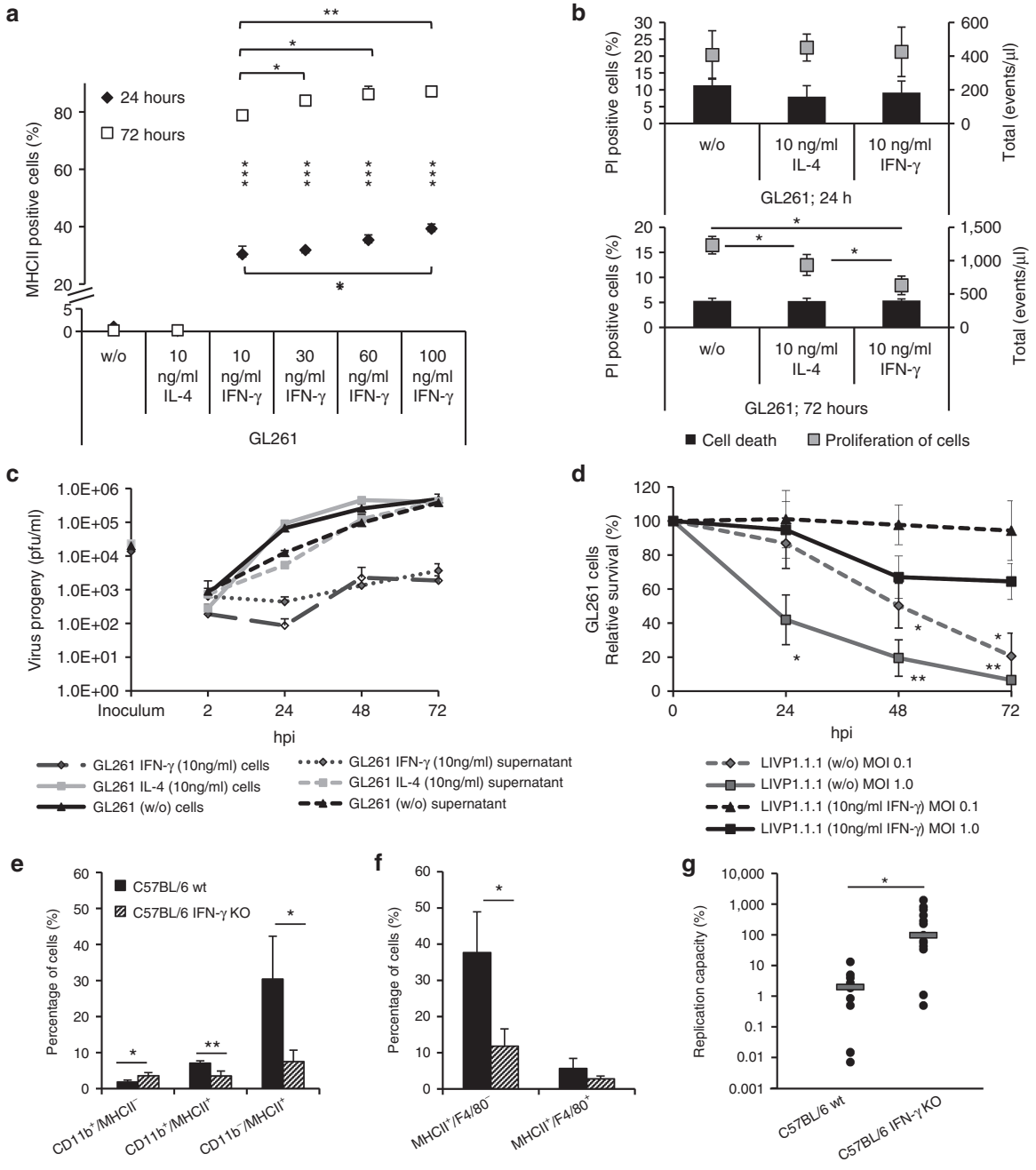

Figure 4 Interferon-γ induced MHCII-upregulation *in vitro* and *in vivo* on GL261 glioma cells and correlated with impaired virus replication and reduced virus-mediated cytotoxicity. MHCII expression on GL261 cells without stimulation (w/o) or after stimulation with 10 ng/ml IL-4 or 10, 30, 60, 100 ng/ml IFN-γ was analyzed by flow cytometry after 24 and 72 hours (**a**). Experiment was performed in triplicates and repeated in an independent experiment. Statistical significance was tested using two-sided *t*-test with unequal variances at each time point (24 and 72 hours) between samples stimulated with 10 ng/ml IFN-γ and 30 ng/ml, 60 ng/ml, or 100 ng IFN-γ, respectively indicated by horizontal asterisk (*$P < 0.05$, **$P < 0.01$, ***$P < 0.001$). In addition, statistical significance was compared for each concentration (10 ng/ml, 30 ng/ml, 60 ng/ml, or 100 ng IFN-γ) between different time points (24 and 72 hours), indicated by vertical asterisk *$P < 0.05$, **$P < 0.01$, ***$P < 0.001$). (**b**) Propidium iodide (PI) staining and thus measuring of cell death of GL261 cells w/o, or stimulated with 10 ng/ml IL-4 or IFN-γ for 24 and 72 hours was determined by flow cytometry. The bar charts represent the mean value and standard deviation of dead cells in percentage. Cell proliferation was determined by measuring the total events per µl until a total of 10,000 "gated" events were reached. Cell debris was excluded from the measurement. (**c**) GL261 cells w/o, or stimulated with IL-4 (10 ng/ml) or IFN-γ (10 ng/ml) for 24 hours were infected with LIVP 1.1.1 at a MOI of 0.1 and viral titers were determined 2, 24, 48, and 72 hpi. The chart shows the mean of triplicate samples and standard deviation. For MTT-assay, GL261 cells were infected with LIVP 1.1.1 (MOI 0.1 and 1.0) (**d**). Experiment was performed in triplicates in two independent experiments. Statistical significance was tested using two-sided t-test with unequal variances, *$P < 0.05$, **$P < 0.01$, ***$P < 0.001$. Flow cytometry analysis of single cell suspensions isolated from s.c. GL261 tumors of C57BL/6 wt and C57BL/6 IFN-γ KO mice on d0 (**e,f**). Shown are mean and standard deviation of four mice per group in percentages (%). Experiment was performed twice in independent set ups. Differences between the mouse strains were tested using two-sided *t*-test with unequal variances. Replication capacity (%) of s.c. Gl261 tumors of C57BL/6 wt ($n = 14$) and C57BL/6 IFN-γ KO mice ($n = 13$) 1 dpi (**g**). Viral titers were determined by plaque assay. The experiment was performed twice in two independent set ups. For the final calculations, the experiments were taken together. Statistical power analysis of the experiment was performed.

of CD11b⁻/MHCII⁺ tumor cells in the single cell suspensions of tumor homogenates from C57BL/6 wt mice over time from day 0 to day 6 (Figure 5a,b). Viral plaque assay of freshly isolated subcutaneous tumor homogenates of C57BL/6 wt mice that were *ex vivo* cultured for 1 day prior to LIVP 1.1.1 infection (MOI 0.1) revealed, that virus titers remained below the virus inoculum 24 hpi (Figure 5c). Tumor homogenates isolated from C57BL/6 wt mice or Balb/c athymic mice *ex vivo* cultured for 6 days supported LIVP 1.1.1 (MOI 0.1) replication 24–72 hpi (Figure 5d) in accordance with a loss of MHCII expression (Figure 5a,b). We further showed, that tumor cells from both mouse strains cultured *ex vivo* for 14 days, and being in a MHCII⁻ status at this time point, upregulated MHCII on their cell surface with an increase from 24 to 72 hours after stimulation with IFN-γ (Figure 5e). These results showed that imprinting of GL261 tumor cells by endogenous IFN-γ levels in C57BL/6 mice is not a permanent effect and tumor

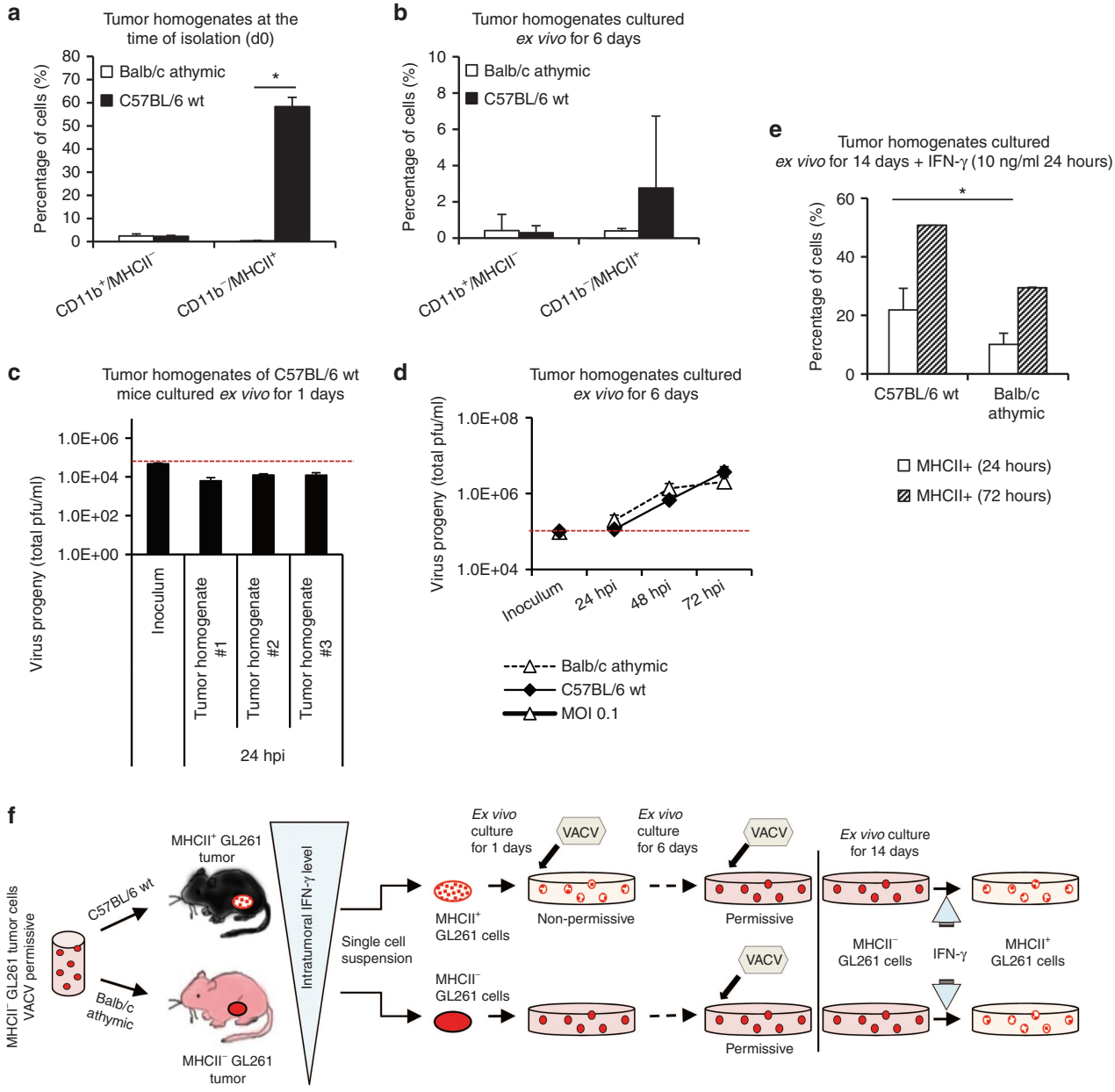

Figure 5 IFN-γ induced antiviral state in GL261 glioma cells is a reversible effect. Single cell suspension of s.c. GL261 tumors of C57BL/6 wt and Balb/c athymic mice were prepared on d0. Flow cytometry analysis was performed on d0 (**a**) and after 6 days of *ex vivo* cultivation (**b**). Shown are the mean values and standard deviation ($n = 3$ mice) of the percentages of CD11b⁺/MHCII⁺ and CD11b⁻/MHCII⁺ immune and tumor cells. Differences between the mouse strains were tested using two-sided *t*-test with unequal variances. (**c**) Tumor homogenates of subcutaneous GL261 allografts isolated from tumors of C57BL/6 wt mice ($n = 3$) were cultured in 24-well plates for 24 hours and infected with LIVP 1.1.1 at a MOI of 0.1. Virus titers were analyzed by standard plaque assay. (**d**) Tumor homogenates of s.c. GL261 allografts isolated from tumors of C57BL/6 wt or Balb/c athymic mice cultured *ex vivo* for 6 days ($n = 3$) were infected with LIVP 1.1.1 (MOI 0.1) and analyzed by standard viral plaque assay in triplicate. Shown are mean values and standard deviation. (**e**) Tumor homogenates from C57BL/6 wt and Balb/c athymic mice were cultured *ex vivo* for 14 days and stimulated for 24 hours with 10 ng/ml IFN-γ. Cells were analyzed by flow cytometry analysis for MHCII expression 24 and 72 hours post stimulation. Shown are mean and standard deviation of three mice per group in percentages (%). Differences between the mouse strains were tested using two-sided *t*-test with unequal variances. (**f**) Schematic overview of the experimental setup and results.

cells can be reset into the status before implantation after cultivation in cell cultures for an appropriate time period (Figure 5f).

DISCUSSION

In the present study, we used a comparative experimental design, considering the genetic background and the immunologic status of the host, to investigate potential microenvironmental factors which are responsible for failure or success of treatment in different GL261 glioma models (Figure 6). In our experimental setup, the genetic background—which is one of the most important determinants in the regulation of immune responses in humans and mice[23]—could be identified to have major impact on VACV LIVP 1.1.1 replication in the subcutaneous GL261 glioma models and thus on the efficacy of oncolytic virotherapy. In case of orthotopic GL261 gliomas located within the brain there are additional cellular factors influencing the success of oncolytic virotherapy in both, C57BL/6 wt and Balb/c athymic mice (submitted manuscript, Kober and Rohn *et al.*). Only Balb/c athymic mice with subcutaneous GL261 tumors supported viral replication (responder) in contrast to mice with C57BL/6 background (non-responder).

In line with our findings are the in detail studied disease mechanisms of ectromelia virus infection, which is the causative agent of mousepox and another member of the *Poxviridae* family.[24,28] C57BL/6 mice are categorized as genetically resistant and Balb/c mice as susceptible mouse strain for mousepox disease.[24,28,34] The strain dependent resistance is controlled by different gene complexes: Exemplary gene complexes are the major histocompatibility complex, the fifth component of complement C5, selectin and natural killer cell genes. The strain dependent resistance is further dependent on the capacity and time-frame of Th1 cytokine production (IFN-γ, IL-2, and IL-12) and antiviral cytotoxic T-lymphocyte response.[24,28] Furthermore, it has been demonstrated, that inhibition of IFN-γ with monoclonal neutralizing antibodies in the resistant C57BL/6 mice resulted in diminished NK and CTL responses and in the development of fulminant mousepox. The course of disease was comparable to susceptible Balb/c mice.[24,34] It is important to note that the studies described above were performed in wild-type mice whereas our study was performed in both wild-type and athymic mice.

Based on the genetic background, which is known to control important immunological functions, we wanted to identify immunological factors in the tumor microenvironment of the subcutaneous tumor models that enabled VACV LIVP 1.1.1 replication on the one hand and prevented replication in mice with C57BL/6 background on the other hand.

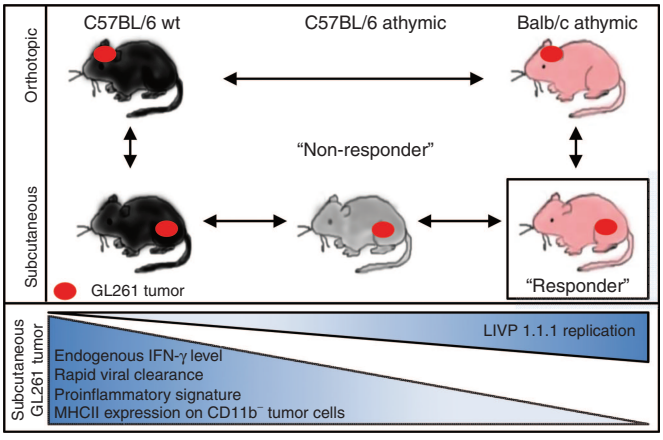

Figure 6 Schematic representation of the comparative experimental setup and key findings within the GL261 glioma model influencing oncolytic virotherapy with VACV LIVP 1.1.1.

By a direct comparison of GL261-tumor-bearing C57BL/6 wt and C57BL/6 IFN-γ KO mice the presence or absence respectively of endogenous IFN-γ in the tumor microenvironment, could be identified as factor responsible for a rapid VACV LIVP 1.1.1 inhibition in the C57BL/6 wt model. IFN-γ (IFN type II) is a proinflammatory cytokine that together with type I IFNs (IFN-α, β) play pivotal role in the control of intracellular pathogens.[31] In case of VACV the two effector enzymes iNOS and IDO, activated downstream of the IFN-γ receptor, were described to directly block virus replication.[35,36] Trilling *et al.*[37] reported that IFN-γ blocks preferentially late gene transcription and VACV genome replication in mouse fibroblasts and target genes of the transcription factor interferon regulatory factor 1 (IRF-1) are crucial for the induction of the antiviral state. Besides direct IFN-γ-induced antiviral effects also the pro-apoptotic and anti-proliferative effects of IFN-γ have impact on viral replication.[31] The interplay between viruses and the interferon system as well as diverse resistance mechanisms such as a soluble IFN-γ receptor expressed by VACV or IFN-γ-binding proteins are summarized in detail in refs. [31,38,39]. IFN-γ also plays an important role in the so called "cancer immunoediting concept" that on the one hand describes the tumor suppressor functions of the immune system and on the other hand the ease of tumor progression by sculpting the immunogenic phenotype of developing tumors and thereafter.[40,41] It is described that tumor formation can be prevented by high endogenous IFN-γ levels of the host. In mice with low endogenous IFN-γ levels like the athymic nude and SCID nude mice it was observed that these mice are more susceptible for tumor formation than wild-type mice (reviewed in ref. 42). This observation is in line with our findings since tumors of athymic mice reached the "time of injection" (tumor volume of 200–400 mm^3) about 7 days faster compared to C57BL/6 wild-type mice. The time of injection in Balb/c athymic mice was 11–13 dpimp, in C57BL/6 athymic mice 12–13 dpimp and in C57BL/6 wt mice 17–21 dpimp. Another explanation for the slower tumor growth and thus later "time of injection" in C57BL/6 wt mice could also be due to residual immunogenicity in these mice. However, as the GL261 glioma cell line is syngeneic with the genetic background of the C57BL/6 wt mice, it can be assumed that this effect is only minimal.

Flow cytometry analysis and RBM ELISA revealed an individual tumor microenvironment and composition of immune cells in the GL261 tumors of the different mouse strains. In addition, the adaptive immune system was observed as main immune modulator responsible for significant differences in wild-type and athymic mice.

Besides a great number of proinflammatory cytokines, we found IP-10 a chemokine induced by IFN-γ[43] with highest concentrations in C57BL/6 wt mice, followed by C57BL/6 athymic and Balb/c athymic mice. The concentration gradient of this cytokine and other proinflammatory cytokines correlated with the diverse expression pattern of MHCII detected on the tumor cells in these mice. The GL261 tumors in the C57BL/6 wt mice with an upregulation of MHCII on the tumor cell surface were associated with a highly proinflammatory signature and demonstrate an immunologically active state. Central to the inflammatory active status is the IFN-γ-signal transducer and activator of transcription (STAT-1)-IRF-1 axis.[44] In the study of Murtas *et al.*,[44] the authors demonstrated a strong correlation between IFN-γ and TNF-α induced IRF-1 activation and

nuclear translocation in connection with different intrinsic properties of the cancer cells. Based on the assumption that different cancer cells have a different sensitivity to respond to stimulation with cytokines,[44] we assume the same is true in case of the sensitivity of the GL261 tumor cells and their response to diverse concentrations of endogenous IFN-γ levels in the tested mouse models. As shown in our study and as described by Murtas *et al.*,[44] this concept can be used to test tumor cell lines in cell culture to make predictions about their responsiveness *in vivo.* The immunologically active tumor phenotype is in contrast to the immunologically silent tumor phenotype described to be associated with immune effector functions resulting in immune mediated tissue destruction and tumor rejection and thus displaying a better prognosis and treatment response- especially for cancer immunotherapy.[18,22,44] Kaplan *et al.*[45] nicely demonstrated that one of the major targets of IFN-γ induced antitumor actions are the tumor cells themselves by enhancing their immunogenicity. Our study is in line with research findings by Liu *et al.*[46] describing the induction of a constitutive antiviral state in tumor cells by a constitutively low secretion of type I IFNs (IFN-α, β) by tumor infiltrating cells. In addition, Monsurrò *et al.*[47] described an intrinsic antiviral state and thus two distinct molecular phenotypes of pancreatic adenocarcinoma cells based on a diverse expression profile of interferon-stimulated genes in these cells.

In our study, we clearly demonstrated that in case of IFN-γ sensitive GL261 tumor cells the success of oncolytic virotherapy with VACV is dependent on the endogenous intratumoral IFN-γ level. We could identify IFN-γ to be responsible not only for the immune-cell-like upregulation of MHCII on the tumor cell surface but also for the induction of an antiviral state in these cells resulting in reduced viral replication and virus-mediated cell death. In the present study, the IFN-γ induced antitumor effects described for the immunological active phenotype do not seem to be strong enough to lead to therapeutic success.

Taken together, this study nicely illustrates that for successful development of cancer therapeutics the genetic and immunologic background of the patient should be taken into account. Further, the concept of personalized medicine and pretesting of patients before starting a particular therapy could be highly advised. One possible biomarker for oncolytic virotherapy of cancer could be the endogenous IFN-γ level or MHCII expression on cancer cells respectively and the sensitivity of the particular cancer type to this cytokine.

MATERIALS AND METHODS

Virus strains

LIVP 1.1.1 was isolated from a wild-type stock of the VACV vaccine strain LIVP originated from the Lister strain (Institute of Viral Preparations, Moscow, Russia). LIVP 1.1.1 represents a "native" virus where no genetic manipulations were conducted. Sequence analysis revealed a naturally occurring disruption of the thymidine kinase (Tk) gene locus.[48] Consequences of a Tk gene deletion in VACVs are a preferential replication in dividing cells such as tumor cells resulting in enhanced tumor specificity and reduced virulence.[49,50] Toxicity and efficiency of LIVP 1.1.1 was tested in various cell lines in cell culture and *in vivo.*[13,51]

Cell lines

African green monkey kidney fibroblast (CV-1) cells were obtained from the American Type Culture Collection (ATCC, Manassas, VA). Murine GL261 glioma cells were kindly provided by A. Pagenstecher (Department of Neuropathology, University Hospital of Marburg, Germany) and the cell line was authenticated by the Leibniz Institute DSMZ (Braunschweig, Germany). CV-1 and GL261, were cultured in Dulbecco's Modified Eagle Medium (DMEM, Sigma-Aldrich, Steinheim, Germany) supplemented with 10% fetal bovine serum (FBS, PAA Laboratories, Coelbe, Germany) and penicillin G/streptomycin solution (100 U/ml, Sigma-Aldrich). Cells were maintained and incubated at 37 °C with 95% humidity and 5% CO_2 and growth medium was changed every third day until confluence.

Cell culture experiments

GL261 cells or single cell suspensions were seeded in wells of a 24-well plate in 1 ml culture medium with 2% FBS supplemented with 10 ng/ml recombinant murine (rm)-IL-4 (ImmunoTools GmbH, Friesoythe, Germany) or rm-IFN-γ (ImmunoTools GmbH, Friesoythe, Germany) or without stimulation (w/o) as control. Twenty-four and 72 hours later, cells were analyzed for the expression of MHCII by flow cytometry or were infected with LIVP 1.1.1 at a MOI of 0.1 for viral replication and MTT-assay, respectively. After infection, cells were either cultured with culture medium (10% FBS) or in culture medium supplemented with the particular cytokine (10 ng/ml). In addition, 30, 60, and 100 ng/ml rm-IFN-γ were used for stimulation of GL261 cells to test MHCII expression by flow cytometry analysis 24 and 48 hours postinfection (hpi).

Flow cytometry analysis of cultured cells

Cells were detached with trypsin/ethylenediaminetetraacetic acid (EDTA, PAA Laboratories, Coelbe, Germany) and centrifuged at 2,000 rpm for 3 minutes. The pellets were resuspended and stained in 200 µl phosphate buffered saline (PBS, PAA, Pasching, Austria) + 2% FBS and 0.2 µl labeled monoclonal antibody anti-mouse MHCII-PE (clone M5/114.15.2, eBioscience, Frankfurt, Germany) for 45–60 minutes at 4 °C. Afterwards, cells were washed once and resuspended in PBS + 2% FBS. To distinguish dead and living cells, 1 µl propidium iodide (PI, Sigma-Aldrich, Steinheim, Germany) was added to the samples 5 minutes prior to measurements. For analysis, an Accuri C6 Cytometer and flow cytometry analysis software CFlow Version 1.0.227.4 (Accuri Cytometers, Ann Arbor, MI) were used. 10,000 events per sample were counted. Experiments were performed in triplicate and repeated twice.

Replication analysis and standard viral plaque assay

Cells were infected with LIVP 1.1.1 (MOI 0.1) diluted in infection medium with 2% FBS for 1 hour. Infection medium was collected and replaced by 1 ml culture medium. Cells were resuspended in 1 ml PBS after harvesting. Supernatants were collected separately 24, 48, and 72 hpi. Prior to analysis three freeze and thaw cycles in liquid nitrogen were accomplished to release viral particles. All samples were infected in triplicate. Serial dilutions of the samples were titrated on 100% confluent CV-1 monolayers in duplicate for standard viral plaque assay. The replication capacity in percentage (%) was calculated by the following formula ((actual viral load (pfu/ml)/virus inoculum (pfu/ml)) * 100%). The initial infection dose (inoculum) was set 100%.

MTT cell viability assay

Cells were infected with LIVP 1.1.1 at a MOI of 0.1 and 1.0. Cell viability was determined 24, 48, and 72 hours after viral infection. For this purpose, culture medium was replaced by 500 µl sterile filtrated 3-(4,5-Dimethylthiazol-2-yl)-2,5-diphenyltetrazolium Bromide (MTT 2.5 mg/ml; Sigma-Aldrich) dissolved in medium without phenol red (Sigma-Aldrich). After an incubation time of 2 hours at 37 °C in the 5% CO2 incubator the MTT-solution was removed. The color reaction and thus the cell viability was measured after adding 400 µl 1 N HCl (Sigma-Aldrich) diluted in isopropyl alcohol (Roth, Karlsruhe, Germany). The optical density was measured at a wavelength of 570 nm in an Elisa Photometer Sunrise (TECAN Group, Männedorf, Germany). Uninfected cells were used as positive control, defined as 100% viable. The experiment was performed two or three times in triplicate.

Animal studies

All animal experiments were carried out in accordance with protocols approved by the Regierung von Unterfranken, Germany (permit number: Az. 55.2-2531.01-30/12 and AZ 55.2-2531.01-62/11).

Subcutaneous implantation of GL261 cells and tumor growth analysis

Five to 6-week-old female Balb/c athymic nude (Hsd:Athymic Nude-*Foxn1*^{nu}), C57BL/6 wt (C57BL/6JOlaHsd) mice ordered from Harlan Winkelmann GmbH (Borchen, Germany), C57BL/6 athymic nude (B6.Cg/NTac-*FoxN1*^{nu}) mice from

Taconic Europe A/S (Lille Skensved, Denmark) and C57BL/6 IFN-γ knockout (KO) (B6.129S7-*Ifngtm1Ts*/J) mice purchased from Charles River Laboratories (Sulzfed, Germany) were implanted subcutaneously (s.c.) with 1×10^6 GL261 cells in 100 µl PBS into the abdominal right hint flank. Tumor growth was monitored every third day. Tumor volume was measured from two directions with a digital caliber and calculated as follows ((length × width2) × 0.52). At a tumor volume between 200–300 mm^3 mice were injected intratumorally (i.t.) with 5×10^6 pfu LIVP 1.1.1 or mock control in a volume of 100 µl PBS.

Orthotopic implantation of GL261 cells

Four to 5-week-old Balb/c athymic and C57BL/6 wt mice were stereotactically implanted intracranially with 1×10^5 GL261 cells. Mice were anesthetized with a mixture of ketamine (Ketavet, Pharmacia GmbH, Berlin, Germany) and xylazine (Xylavet, CP-Pharma GmbH, Burgdorf Germany) by intraperitoneal (i.p.) injection. Mice were placed and fixed in a stereotactic apparatus (Stoelting Europe, Dublin, Ireland) and tumor cells in a volume of 2 µl were injected 2.0 mm in depth over a period of 5 minutes (0.5µl/minute) 1.0 mm anterior and 2.0 mm lateral to the bregma with a Hamilton syringe (A. Hartenstein Gesellschaft für Labor- und Medizintechnik GmbH, Wuerzburg, Germany). The incision was closed with surgical stables and Metacam (Boehringer Ingelheim, Ingelheim, Germany) was administered (s.c.) for analgesia. 15–17 days post implantation (dpimp) in C57BL/6 wt and 14 dpimp in Balb/c athymic mice 5×10^6 pfu LIVP 1.1.1 in 3 µl PBS (~ 0.5 µl/min) were injected intracranially into the implantation site over a period of 5 minutes. Mice were treated similar as for the tumor cell implantation.

Determination of VACV titer in subcutaneous and orthotopic GL261 tumors

Mice with subcutaneously or orthotopically grown GL261 tumors were euthanized at day 1 or 7 post virus infection. Tumors/brains were excised, weighed and transferred into 1.4 mm ceramic bead tubes (Peqlab; Erlangen, Germany) containing 1 ml of PBS. Tumors/brains were mechanically homogenized with a FastPrep Cell Disruptor (Thermo Scientific, Karlsruhe, Germany). Samples were centrifuged at 13,000 rpm for 4 minutes. Supernatants were freeze-thawed three times and then analyzed by standard viral plaque assay. The unit (pfu/g tissue) represents the viral titer (pfu) in proportion to the tumor weight (g) of the tumor or tissue on the day the tumor was harvested (1 or 7 dpi).

Rodent multi-analyte profile

To prepare tumor lysates at the "day of potential infection" (d0) five mice of each mouse strain (Balb/c athymic, C57BL/6 wt and athymic) with subcutaneous GL261 tumor were sacrificed. Tumors were crushed and resuspended in 9 volumes of ice cold lysis buffer consisting of 50 mmol/l Tris-HCl (pH 7.4), 2 mmol/l EDTA (pH 7.4), 2 mmol/l PMSF and Complete Mini protease inhibitors (Roche, Mannheim, Germany) and lysed in a gentleMACS Dissociator using M-Tubes (both Miltenyi Biotec GmbH, Bergisch Gladbach, Germany). Tumor samples were centrifuged at 13,000 rpm for 5 minutes at 4 °C and supernatants were analyzed by Myriad RBM (Austin, TX) for an immune-related protein antigen profiling (RodentMAP v. 3.0).

Clodronate depletion

C57BL/6 wt mice were implanted subcutaneously with 1×10^6 GL261 cells. When tumors reached a size between 200–400 mm^3, mice were i.p. injected on three consecutive days with 200 µl clodronate liposomes (Clodronate liposomes in 10 ml PBS; ClodronateLiposomes.com, Haarlem, The Netherlands) or PBS. On day 4 after these injections, tumors were i.t. injected with LIVP 1.1.1 (5×10^6 pfu) for analysis with standard viral plaque assay and flow cytometry.

Preparation of single cell suspensions from subcutaneous tumors

For flow cytometry analysis or cell culture studies, 3–4 C57BL/6 wt, C57BL/6 athymic, Balb/c athymic, or C57BL/6 IFN-γ-KO mice were sacrificed by CO_2-inhalation on d0 or 1 dpi. Blood was taken and tumors were removed. Single cell suspensions of tumors were prepared as described by Gentschev *et al.*[10] In brief, tumor tissues were minced and transferred into a 50 ml tube containing 5 ml Roswell Park Memorial Institute (RPMI, Sigma-Aldrich) + 2% FBS, 150 µl 10,000 CDU/ml Collagenase I (Sigma-Aldrich) and 5 µl 5 MU/ml DNase I (Calbiochem, Darmstadt, Germany) for 40 minutes at 37 °C. Afterwards, cells were passed through a 70 µm nylon mesh filter (BD Biosciences, Erembodegem, Belgium). Suspension was centrifuged at 1,000 rpm for 10 minutes and washed once with 20 ml PBS + 2% FBS. For the blood samples, 0.1 ml blood/2 ml 1× lysis buffer (10× stock: 8.29 g NH_4CL + 1.09 g $KHCO_3$ + 41 mg EDTA-NA_2 dissolved in 100 ml H_20) were incubated for 10 minutes at RT. The samples were then centrifuged at 1,200 rpm for 5 minutes and washed twice.

Flow cytometry of single cell suspensions of tumor homogenates

Cell suspensions were blocked with purified anti-mouse CD16/CD32 (1 µl/1×10^6 cells) (clone 93; eBioscience, Frankfurt, Germany) for 30 minutes at 4 °C. Cells were stained in appropriate antibody solutions for 40 minutes at 4 °C. The following monoclonal anti-mouse antibodies were used in this study: CD3-PE (clone145-2C11; eBioscience), CD4-APC (clone GK1.5; eBioscience) CD8-FITC (clone 53-6.7: BD Bioscience Heidelberg, Germany), CD11b-APC (clone M1/70; eBioscience), CD11b-PE (M1/70; BD Biosciences), CD11b-PerCP-Cyanine5.5 (clone M1/70; eBioscience), CD14-PerCP (clone Sa2-8; eBioscience), Ly6c-PerCP-Cy5.5 (AL-21; BD Bioscience, Heidelberg, Germany), Gr1-FITC (clone RB6-8C5; eBioscience), CD49b-APC (clone DX5; eBioscience), CD19-PerCP/Cy5.5 (clone 6D5; eBioscience), CD11c-Pe and CD11c-APC (clone N418; BioLegend, London, UK), Ly6G-PE (clone 1A8; BD Biosciences), CD45-PerCP-Cy5.5 (clone 30-F11; eBioscience), MHCII-PE (clone M5/114.15.2; eBioscience, F4/80-APC (clone BM8; eBioscience). The following isotype controls have been used: Rat IgG2a K-PE/APC/FITC/PerCP-Cy5.5 (clone eBR2a; eBioscience), Rat-IgG2b K- PE/APC/FITC/PerCP-Cy5.5 (clone eB149/10H5; eBioscience), Hamster IgG-APC (clone HTK888; BioLegend, London, UK), Rat-IgM-APC (eBioscience), Rat-IgG1-APC (clone EBRG1; eBiosience). For the intracellular staining of CD68 and CD206 cells were fixed with 2% paraformaldehyde/PBS solution (Applichem, Darmstadt, Germany) for 15 minutes at RT under continuous agitation. The reaction was stopped with PBS + 2% FBS. Afterwards CD206-FITC (clone C068C2, BioLegend) or CD68-FITC (Serotec, Puchheim, Germany) were diluted in permeabilization buffer (5% FBS, 0.1% NaN_3, 0.2% Saponin in PBS) in the appropriate concentration and stained for 1 hour at 4 °C. Prior to the analysis, cells were washed once and resuspended in an appropriate volume of PBS + 2% FBS. Stained cells were analyzed using an Accuri C6 Cytometer and flow cytometry analysis software CFlow Version 1.0.227.4 (Accuri Cytometers). 10,000 events per sample were analyzed. Cell debris was excluded by FSC/SSC gating. Double stainings were conducted to avoid false positive or unspecific results. Calculated percentages below 1% were defined as not detectable (<1).

Immunohistochemistry of cryosections

For immunohistochemistry, mice were sacrificed by CO_2 inhalation. Tumors were excised and snap frozen in liquid nitrogen. Fixation, embedding and sectioning were performed as described in ref. 11. Slides were fixed in ice-cold acetone for 10 min and afterwards stained with anti-mouse MHC class II (I-A/I-E) or anti-mouse MHC class II ((I-A/I-E) functional grade biotin (clone M5/114.15.2; eBioscience) and rat-anti-mouse CD68 (FA-11; Serotec) in single or costainings for 1 hour at RT. After three washing steps with PBS, sections were labeled with secondary antibodies (Cy3/Cy2-conjugated AffinityPure Donkey Anti-Rat IgG (H+L); Jackson ImmunoResearch Laboratories. West Grove, PA) Streptavidin-Cy3 (from *Streptomyces avidinii*, buffered aqueous solution; Sigma-Aldrich) and Hoechst 33258 (Sigma-Aldrich) for 1 hour at RT. After three washing steps and an ethanol step, the slides were mounted in Mowiol 4-88 (Roth, Karlsruhe, Germany). Images were taken at an Axiovert 200M inverse microscope (Zeiss, Jena, Germany) and edited with the software program Axiovison 4.8.2 (Zeiss, Feldbach, Switzerland). Ten images per tumor slice (five images from tumor rim and five from tumor center) were taken at a magnification of 20× with identical settings. RGB-Images were converted into 8-bit gray scale images and the fluorescence intensity of CD68 and MHCII stainings was measured by Image J and represents the average brightness of staining related pixels.

Immunohistochemistry of agarose sections

Brains were excised and snap-frozen in liquid nitrogen, fixed in 4% paraformaldehyde/PBS (pH 7.4, o/n at 4 °C), rinsed with PBS and embedded in 5% low-melting agarose (Sigma-Aldrich). Brains were cut in sections (100 µm) using the Leica VT1000S Vibratome (Leica, Heerbrugg, Switzerland) and blocked in blocking solution (PBS, 0.3% Triton X-100, 5% FBS) for 1 hour. The sections were labeled with the primary antibodies anti-Iba-1 (WEP0389, WAKO, Neuss, Germany) and anti-MHCII (I-A/I-E) functional grade biotin for 12–15 hours. After three washing steps in PBS, sections

were incubated with the secondary antibodies (Streptavidin-Cy3 and donkey anti-rabbit-Cy5; Dianova, Hamburg, Germany) for 5 hours. Nuclei were Hoechst 33342-labeled. Then, sections were washed with PBS and mounted onto glass slides in Mowiol 4-88. The fluorescent-labeled preparations were examined using the MZ16 FA Stereo-Fluorescence microscope (Leica, Wetzlar, Germany) equipped with a digital CCD camera (DC500, Leica, Wetzlar, Germany). The Iba-1-Cy5 staining was converted to a green signal by Photoshop CS5 (Adobe Systems).

Statistics

To determine significance between two independent groups and normal distribution, a two-tailed *t*-test with unequal variances was used (Excel 2010 for Windows). *P* values were defined as follows $*P < 0.05$, $**P < 0.01$, $***P < 0.001$. For calculating boxplot diagrams, a template from Vertex42 LLC has been used. The optimal sample size ($n = 17$) to detect a difference of $d = 1.02$ for the viral replication in C57BL/6 wt and C57BL/6 IFN-γ KO mice was calculated to assure an adequate power to detect statistical significance. We used a power of 80% and an α-level of 0.05. Power analysis was performed using the software G*Power.

CONFLICT OF INTEREST

This work was supported by Genelux Corporation, graduate stipends from the University of Wuerzburg (to C.K. and L.K.) and a postdoctoral fellowship (to S.W. and S.R.) from a Research Service Grant awarded by Genelux Corporation to the University of Wuerzburg. A.A.S. was during the first part of the study, salaried employee of Genelux Corporation and has personal financial interest in Genelux Corporation. The funders had no role in study design, data collection, and analysis or decision to publish.

ACKNOWLEDGMENTS

The authors thank Nanhai G. Chen and Jason Aguilar (Genelux Corporation) for virus preparation, Johanna Langbein-Laugwitz (Department of Biochemistry, University of Wuerzburg) for excellent technical assistance, Saskia Wittber (Department of Biochemistry, University of Wuerzburg) for animal care and Barbara Härtl, Ivaylo Gentschev, Juliane Meir, Sandeep Patil, Marion Adelfinger, Alexander Cecil, (Department of Biochemistry, University of Wuerzburg) and Boris Minev (Genelux Corporation) for helpful discussions. The authors also thank Axel Pagenstecher (Department of Neuropathology, University Hospital of Marburg) for providing the cell line GL261. The study was supported by grants from Genelux Corporation (R&D facility in San Diego, CA, USA) awarded to the University of Wuerzburg and the University of Wuerzburg.

REFERENCES

1. Ohgaki, H and Kleihues, P (2005). Epidemiology and etiology of gliomas. *Acta Neuropathol* **109**: 93–108.
2. Wen, PY and Kesari, S (2008). Malignant gliomas in adults. *N Engl J Med* **359**: 492–507.
3. Patel, MM, Goyal, BR, Bhadada, SV, Bhatt, JS and Amin, AF (2009). Getting into the brain: approaches to enhance brain drug delivery. *CNS Drugs* **23**: 35–58.
4. Adamson, C, Kanu, OO, Mehta, AI, Di, C, Lin, N, Mattox, AK *et al.* (2009). Glioblastoma multiforme: a review of where we have been and where we are going. *Expert Opin Investig Drugs* **18**: 1061–1083.
5. Selznick, LA, Shamji, MF, Fecci, P, Gromeier, M, Friedman, AH and Sampson, J (2008). Molecular strategies for the treatment of malignant glioma-genes, viruses, and vaccines. *Neurosurg Rev* **31**: 141–155.
6. Lun, X, Chan, J, Zhou, H, Sun, B, Kelly, JJ, Stechishin, OO *et al.* (2010). Efficacy and safety/toxicity study of recombinant vaccinia virus JX-594 in two immunocompetent animal models of glioma. *Mol Ther* **18**: 1927–1936.
7. Chen, NG and Szalay, AA. Oncolytic virotherapy in cancer. In: Minev BR (ed.). *Cancer Manag. Man Chemother. Biol. Ther. Hyperth. Support. Meas*. Springer, New York, New York, NY, 2011. pp. 295–316.
8. Kirn, DH and Thorne, SH (2009). Targeted and armed oncolytic poxviruses: a novel multimechanistic therapeutic class for cancer. *Nat Rev Cancer* **9**: 64–71.
9. Chen, NG and Szalay, AA (2010). Oncolytic vaccinia virus: a theranostic agent for cancer. *Future Virol* **5**: 763–784.
10. Gentschev, I, Müller, M, Adelfinger, M, Weibel, S, Grummt, F, Zimmermann, M *et al.* (2011). Efficient colonization and therapy of human hepatocellular carcinoma (HCC) using the oncolytic vaccinia virus strain GLV-1h68. *PLoS ONE* **6**: e22069.
11. Weibel, S, Hofmann, E, Basse-Luesebrink, TC, Donat, U, Seubert, C, Adelfinger, M *et al.* (2013). Treatment of malignant effusion by oncolytic virotherapy in an experimental subcutaneous xenograft model of lung cancer. *J Transl Med* **11**: 106.
12. Donat, U, Rother, J, Schäfer, S, Hess, M, Härtl, B, Kober, C *et al.* (2014). Characterization of metastasis formation and virotherapy in the human C33A cervical cancer model. *PLoS ONE* **9**: e98533.
13. Advani, SJ, Buckel, L, Chen, NG, Scanderbeg, DJ, Geissinger, U, Zhang, Q *et al.* (2012). Preferential replication of systemically delivered oncolytic vaccinia virus in focally irradiated glioma xenografts. *Clin Cancer Res* **18**: 2579–2590.
14. Zemp, FJ, Corredor, JC, Lun, X, Muruve, DA and Forsyth, PA (2010). Oncolytic viruses as experimental treatments for malignant gliomas: using a scourge to treat a devil. *Cytokine Growth Factor Rev* **21**: 103–117.
15. Wollmann, G, Ozduman, K and van den Pol, AN (2012). Oncolytic virus therapy for glioblastoma multiforme: concepts and candidates. *Cancer J* **18**: 69–81.
16. Kaur, B and Chiocca, EA (2007). Personalizing oncolytic virotherapy? *Mol Ther* **15**: 6–7.
17. Ogino, S, Galon, J, Fuchs, CS and Dranoff, G (2012). Cancer immunology - analysis of host and tumor factors for personalized medicine. *Nat Rev Clin Oncol* **8**: 617–632.
18. Galon, J, Angell, HK, Bedognetti, D and Marincola, FM (2013). The continuum of cancer immunosurveillance: prognostic, predictive, and mechanistic signatures. *Immunity* **39**: 11–26.
19. Angell, H and Galon, J (2013). From the immune contexture to the Immunoscore: the role of prognostic and predictive immune markers in cancer. *Curr Opin Immunol* **25**: 261–267.
20. Fridman, WH, Pagès, F, Sautès-Fridman, C and Galon, J (2012). The immune contexture in human tumours: impact on clinical outcome. *Nat Rev Cancer* **12**: 298–306.
21. Allen, M and Louise Jones, J (2011). Jekyll and Hyde: the role of the microenvironment on the progression of cancer. *J Pathol* **223**: 162–176.
22. Ascierto, ML, De Giorgi, V, Liu, Q, Bedognetti, D, Spivey, TL, Murtas, D *et al.* (2011). An immunologic portrait of cancer. *J Transl Med* **9**: 146.
23. Kuroda, E, Noguchi, J, Doi, T, Uematsu, S, Akira, S and Yamashita, U (2007). IL-3 is an important differentiation factor for the development of prostaglandin E2-producing macrophages between C57BL/6 and BALB/c mice. *Eur J Immunol* **37**: 2185–2195.
24. Karupiah, G (1998). Type 1 and type 2 cytokines in antiviral defense. *Vet Immunol Immunopathol* **63**: 105–109.
25. Kuroda, E, Kito, T and Yamashita, U (2002). Reduced expression of STAT4 and IFN-gamma in macrophages from BALB/c mice. *J Immunol* **168**: 5477–5482.
26. Watanabe, H, Numata, K, Ito, T, Takagi, K and Matsukawa, A (2004). Innate immune response in Th1- and Th2-dominant mouse strains. *Shock* **22**: 460–466.
27. Mills, CD, Kincaid, K, Alt, JM, Heilman, MJ and Hill, AM (2000). M-1/M-2 macrophages and the Th1/Th2 paradigm. *J Immunol* **164**: 6166–6173.
28. Szulc, L, Gierynska, M, Winnicka, A, Martyniszyn, L, Boratynska-Jasinska, A and Niemialtowski, M (2012). T cell cytokine synthesis at the single-cell level in BALB/c and C57BL/6 mice infected with ectromelia virus. *Postepy Hig Med Dosw (Online)* **66**: 222–230.
29. http://www.rbm.myriad.com/products-services/biomarker-detail/. 2014.
30. Soos, JM, Krieger, JI, Stüve, O, King, CL, Patarroyo, JC, Aldape, K *et al.* (2001). Malignant glioma cells use MHC class II transactivator (CIITA) promoters III and IV to direct IFN-gamma-inducible CIITA expression and can function as nonprofessional antigen presenting cells in endocytic processing and CD4(+) T-cell activation. *Glia* **36**: 391–405.
31. Schroder, K, Hertzog, PJ, Ravasi, T and Hume, DA (2004). Interferon-gamma: an overview of signals, mechanisms and functions. *J Leukoc Biol* **75**: 163–189.
32. Maes, W and Van Gool, SW (2011). Experimental immunotherapy for malignant glioma: lessons from two decades of research in the GL261 model. *Cancer Immunol Immunother* **60**: 153–160.
33. Weisser, SB, van Rooijen, N and Sly, LM (2012). Depletion and reconstitution of macrophages in mice. *J Vis Exp* **66**: 4105.
34. Chaudhri, G, Panchanathan, V, Buller, RM, van den Eertwegh, AJ, Claassen, E, Zhou, J *et al.* (2004). Polarized type 1 cytokine response and cell-mediated immunity determine genetic resistance to mousepox. *Proc Natl Acad Sci USA* **101**: 9057–9062.
35. Karupiah, G, Xie, QW, Buller, RM, Nathan, C, Duarte, C and MacMicking, JD (1993). Inhibition of viral replication by interferon-gamma-induced nitric oxide synthase. *Science* **261**: 1445–1448.
36. Terajima, M and Leporati, AM (2005). Role of Indoleamine 2,3-Dioxygenase in Antiviral Activity of Interferon-gamma Against Vaccinia Virus. *Viral Immunol* **18**: 722–729.
37. Trilling, M, Le, VT, Zimmermann, A, Ludwig, H, Pfeffer, K, Sutter, G *et al.* (2009). Gamma interferon-induced interferon regulatory factor 1-dependent antiviral response inhibits vaccinia virus replication in mouse but not human fibroblasts. *J Virol* **83**: 3684–3695.
38. Chesler, DA and Reiss, CS (2002). The role of IFN-gamma in immune responses to viral infections of the central nervous system. *Cytokine Growth Factor Rev* **13**: 441–454.
39. Randall, RE and Goodbourn, S (2008). Interferons and viruses: an interplay between induction, signalling, antiviral responses and virus countermeasures. *J Gen Virol* **89**(Pt 1): 1–47.
40. Ikeda, H, Old, LJ and Schreiber, RD (2002). The roles of IFN gamma in protection against tumor development and cancer immunoediting. *Cytokine Growth Factor Rev* **13**: 95–109.
41. Schreiber, RD, Old, LJ and Smyth, MJ (2011). Cancer immunoediting: integrating immunity's roles in cancer suppression and promotion. *Science* **331**: 1565–1570.
42. Manjili, HM (2011). Revisiting cancer immunoediting by understanding cancer immune complexity. *J Pathol* **224**: 5–9.

43. Neville, LF, Mathiak, G and Bagasra, O (1997). The immunobiology of interferon-gamma inducible protein 10 kD (IP-10): a novel, pleiotropic member of the C-X-C chemokine superfamily. *Cytokine Growth Factor Rev* **8**: 207–219.
44. Murtas, D, Maric, D, De Giorgi, V, Reinboth, J, Worschech, A, Fetsch, P *et al*. (2013). IRF-1 responsiveness to IFN-? predicts different cancer immune phenotypes. *Br J Cancer* **109**: 76–82.
45. Kaplan, DH, Shankaran, V, Dighe, AS, Stockert, E, Aguet, M, Old, LJ and Schreiber, RD (1998). Demonstration of an interferon y-dependent tumor surveillance system in immunocompetent mice. *Proc Natl Acad Sci USA* **95**: 7556–7561.
46. Liu, YP, Suksanpaisan, L, Steele, MB, Russell, SJ and Peng, KW (2013). Induction of antiviral genes by the tumor microenvironment confers resistance to virotherapy. *Sci Rep* **3**: 2375.
47. Monsurrò, V, Beghelli, S, Wang, R, Barbi, S, Coin, S, Di Pasquale, G *et al*. (2010). Anti-viral state segregates two molecular phenotypes of pancreatic adenocarcinoma: potential relevance for adenoviral gene therapy. *J Transl Med* **8**: 10.
48. Chen, N.G., Zhang, Q, Yu, Y.A., Szalay, A.A. Vaccinia virus LIVP subclones: Comparative genomic features. 2015, (manuscript in preparation).
49. Zhang, Q, Liang, C, Yu, YA, Chen, N, Dandekar, T and Szalay, AA (2009). The highly attenuated oncolytic recombinant vaccinia virus GLV-1h68: comparative genomic features and the contribution of F14.5L inactivation. *Mol Genet Genomics* **282**: 417–435.
50. McCart, JA, Ward, JM, Lee, J, Hu, Y, Alexander, HR, Libutti, SK *et al*. (2001). Systemic cancer therapy with a tumor-selective vaccinia virus mutant lacking thymidine kinase and vaccinia growth factor genes. *Cancer Res* **61**: 8751–8757.
51. Gentschev, I, Adelfinger, M, Josupeit, R, Rudolph, S, Ehrig, K, Donat, U *et al*. (2012). Preclinical evaluation of oncolytic vaccinia virus for therapy of canine soft tissue sarcoma. *PLoS ONE* **7**: e37239.